ISSN 1064-2293, Eurasian Soil Science, 2022. © Pleiades Publishing, Ltd., 2022.

SOIL PHYSICS

Assessment of the Capability of Satellite Images in Determining the Topsoil Moisture Content in the Dust Hotspot of Southeastern Ahvaz in Iran

F. Hezarian[a], B. Khalilimoghadam[a], A. Zoratipour[b, *], M. Firoozy Nejad[c], and A. Yusefi[a]

[a] *Department of Soil Science, Agricultural Sciences and Natural Resources University of Khuzestan, Mollasani, Iran*
[b] *Department of Nature Engineering, Agricultural Sciences and Natural Resources University of Khuzestan, Mollasani, Iran*
[c] *PhD Candidate, Department of Forestry and Forest Economics, University of Tehran, Karaj, Iran*
**e-mail: Zoratipour@asnrukh.ac.ir*

Received May 4, 2022; revised May 27, 2022; accepted June 30, 2022

Abstract—Soil moisture content is one of the critical parameters in water resource studies and watershed management. Large-scale field measurement is a tough, time-consuming, and costly task. newly, models based on remote sensing indicators have found special importance with high accuracy to investigate the soil and water resources. This study aims to use Landsat 8 satellite imagery to study variation in topsoil moisture content of dust hotspots of southeastern Ahvaz of Iran, over the five months (from February to June 2019). After monthly field sampling, satellite images were applied to determine the NDMI index and the topsoil moisture content using Bands 5 and 6 (main Bands) of Landsat 8 satellites. Then, by fusion, with Band 8 (panchromatic Band), the soil moisture content map was obtained for each month. The Pearson correlation positive was obtained between the NDMI of the main band and the NDMI of fusion with the soil moisture content of field for April month, with a correlation coefficient 0.543, and a significance level of 0.05 (P-value < 0.05). Also, for each month, the humidity index modeling was obtained for both data (the main (original) band and the fusion band). The proposed model was evaluated using statistical metrics namely R2, RMSE and MAE to April month, and the results were 0.57, 1.25 and 5.45, respectively. After validating the models, the best ones were selected for estimating the soil moisture content. Finally, the obtained results showed that Landsat 8 data presented satisfying outcomes for estimating map soil moisture content.

Keywords: Soil moisture content, dust storm, NDMI, LANDSAT 8
DOI: 10.1134/S106422932211014X

INTRODUCTION

The topsoil moisture content is one of the most important environmental variables in climatic, ecological, and hydrological models [4]. Wind erosion in arid and semi-arid climates causes tremendous and irreparable damage. Soil moisture content has a prominent role in controlling wind erodibility so that with increasing soil moisture, the rate of wind erosion decreases outstandingly [18]. In other words, low soil moisture content has low adhesion and is therefore prone to erosion; so, dry soils are prone to dust hotspots [13]. Considering that the study area is based on the De-Martonne Index (which consists of two variables of average rainfall and average maximum temperature, nearly 180 mm and 51°C), it has an arid climate. Also, Khuzestan is facing many problems regarding water resources shortage. So, the accurate estimation of the temporal and spatial variations of topsoil moisture content can be effective in controlling the desertification phenomenon and achieving sustainable development in the region [11]. Remote sensing methods can be applied to estimate soil moisture content on a large scale [5]. Since, the vegetation plays a significant role in stabilizing the soil and preventing erosion, the loss of this coverage has a significant part in desertification and the formation of dust. Yuan et al., monitored topsoil moisture content changes for 18 years using data from the TM[1] and ETM[2] dual sensors. The results showed a direct linear relationship between TDVI[3] and surface soil moisture content [21]. Also, for estimating the topsoil moisture content, Khanmohammadi and Homaee, carried out a study using NDVI[4] and LST[5] indices and using MODIS satellite images [12]. After calculating the topsoil moisture content model, the results showed an acceptable correlation (66%) between topsoil moisture content

[1] Thematic Mapper.
[2] Enhancing Thematic Mapper.
[3] Transformed Difference Vegetation Index.
[4] Normalized Difference Vegetation Index.
[5] Land Surface Temperature.

values with NDVI, NDMI[6], and LST indices [12]. Le and Liou, estimated soil moisture content with Landsat data in Jiangsu, Hunan and Sichuan provinces. In that study, time-series images were used for soil surface moisture (volumetric) at 30 meters. The results showed that the obtained models agreed with the ground measurements [14]. Şekerte kin et al., mapped soil moisture content using Sentinel 1A satellite imagery and found Sentinel data reasonably accurate for estimating and mapping soil [20]. Finally, the estimated model was evaluated using statistical coefficients of (R2) and (RMSE), and the results were 0.84 and 2.46%, respectively [20]. Rawat et al., conducted a study to compare soil moisture content using Landsat 8 and Sentinel satellite imagery with the TDR method (TDR, is tool used to obtain the actual soil moisture content) [19]. The statistical experiments showed a suitable accuracy between soil moisture content observed and estimated using satellite data. Since, different regions of southern Khuzestan province are facing many problems of water resources shortage, the expansion of studies regarding of accurate estimation of soil moisture content is of particular importance. Therefore, the existence of reliable models for calculating the surface soil moisture content with the spatial and temporal proper distribution and low cost is essential. In addition, the prone areas to dust production in Khuzestan province are located in the southeastern, southern and western parts of the province. Despite the conducted research, not much information is available about the exact location and temporal and spatial changes of topsoil moisture content the region. The objective of this study was to estimate topsoil moisture content map, using Landsat 8 satellite images in dust hotspots in Khuzestan province and, determine whether,

(a) Are the remote sensing indices capability monitoring the temporal and spatial changes of topsoil moisture content in arid regions of Iran?

(b) Is the accuracy of monitoring the temporal and spatial changes of soil surface moisture in the different months of the year? Which months are more accurate in arid regions of Iran?

(c) Is effective the combination of the 5 and 6 bands (main bands) with 8 band or panchromatic (Fusion images) increasing the accuracy of the topsoil moisture content map?

OBJECTS AND METHODS

Study Area

The area of this research is located in the dust hotspot of the south-eastern Ahvaz, which starts from 25 km southeast of Ahvaz and along the Ahvaz-Mahshahr freeway (geographical coordinates 48°47′, to 49°17′ E and 30°45′, to 31°15′ N). This region is one of the leading centres of dust storms [17] in Khuzestan province (centre number four) (Fig. 1a). The annual precipitation and temperature in the region are approximately 180 mm and 25°C, respectively, and most precipitation falls in January month. Also, the absolute maximum temperature in the south-eastern Ahvaz is between 52° in the west to 51.7° in the east. The elevation variation of the area is from 8 to 24 m. Accordingly indicated by the De-Martonne Index classification, this region has an arid climate and is situated [10, 17].

Soil texture affects many physical and chemical properties of soil. According to the field studies, the results showed that the dominant soil textures was clay and clay loam. Soils have high salinity with an average of 15 to more than 70 dS/m, with high erodibility (Table 1). The land cover was determined systematic-randomly in the field, by cutting and weighing method (one square meter plots) in every land unit. There are four types of land cover in the case study, which include water surface, scarce vegetation, bare uncultivated land and cropland (Fig. 1b). The average slope of the area is less than 0.02 percent and the lands are flat, and the region has few elevation changes. The percentage of vegetation was less than 5 percent (Fig. 2). The groundwater depth is estimated at 3 to 4 meters. The study area is divided into 27 land units (Table 1) based on land use, topography, and geological formations factors [1], (Fig. 2). In each land unit, at least 3 points were randomly selected, and at each land unit, soil samples were taken from the soil surface (0–20 cm) in three replications and were transferred to the laboratory.

Soil Attributes

Particle size distribution (PSD) was determined by sieving and sedimentation, and aggregate stability was measured by dry sieving. Soil moisture content percentage and moisture content at permanent wilting point (PWP) were measured using the gravimetric method and the pressure plate apparatus, respectively [9]. The Walkley–Black method measured organic carbon. The pH of saturated paste using a Jenway pH meter at 25°C. The calcium carbonate equivalent (CCE) was determined using the HCl back-titration method [9, 10]. Electrical conductivity (EC) was measured in a saturated paste using a Jenway EC meter (Cole-Parmer, Staffordshire, UK) at 25°C. The sodium adsorption ratio (SAR) was calculated by the standard method [9, 10].

Soil Moisture Content

In this study, ground measurements were made from a depth of 0–20 cm, and monthly samples (243 samples monthly, included 27 units' land * three points * three replications) were taken. After transferring the samples to the laboratory, was obtained their moisture content

[6] Normalized Difference Moisture Index.

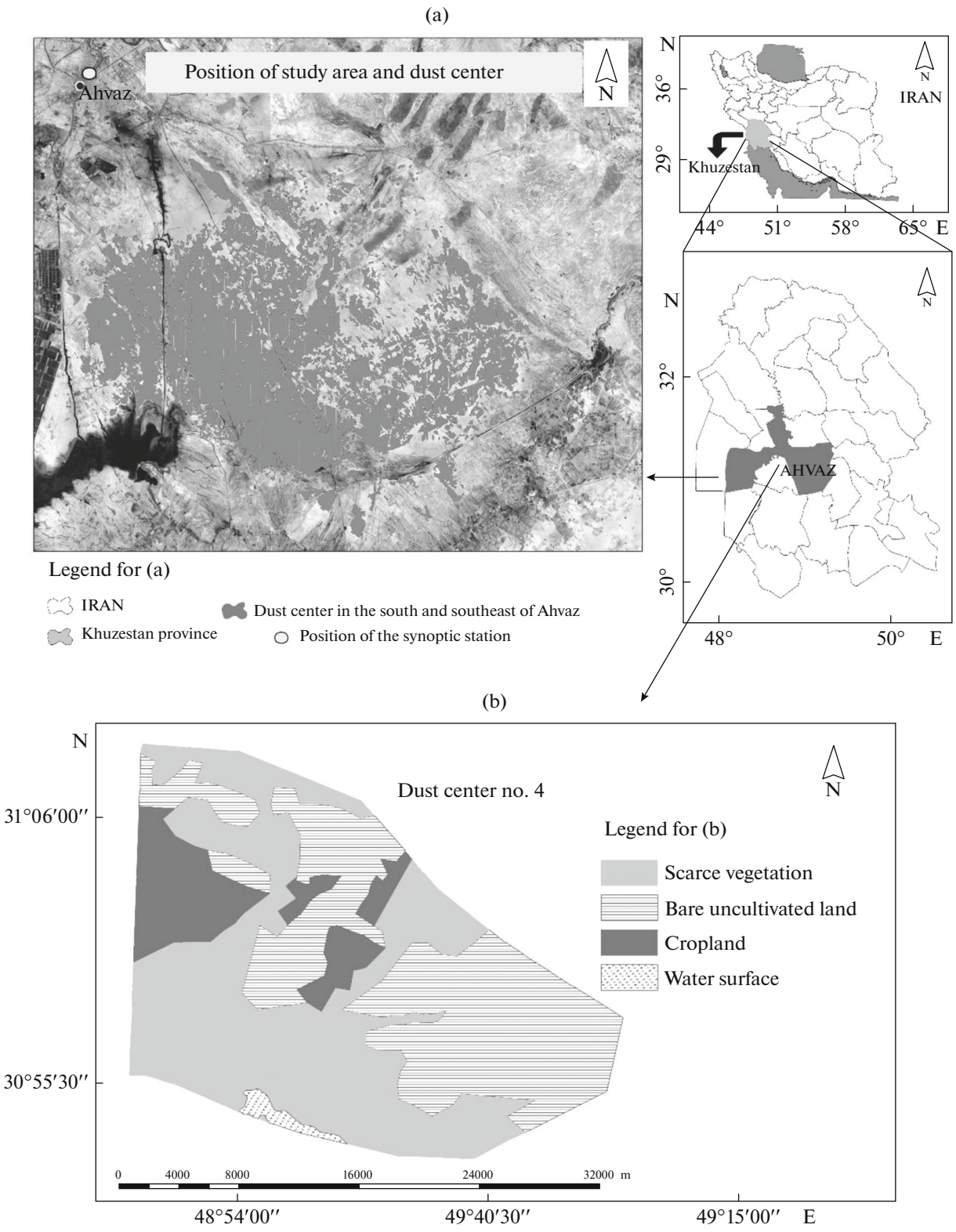

Fig. 1. Fig. (a) study area and dust Hotspot and Fig. (b) Dust hotspot no. 4 in Khuzestan province.

Table 1. Soil surface (<20 cm) properties of different land types and land units in the study area

Land type	Land unit	Area, ha	Texture	EC, dS m^{-1}	OM, %	SAR	Vegetation cover, %
5	5.1.1	190	Clay	5.2 ± 4.1	0.29 ± 0.4	2.1 ± 1.5	8 ± 4
	5.1.2	214	Loam	19 ± 12.2	0.25 ± 0.24	53.6 ± 12.5	10 ± 5
	5.1.3	493	Clay	35 ± 12.0	0.38 ± 0.12	105.2 ± 15.6	5 ± 3
	5.1.4	322	Loam	16 ± 8.4	0.38 ± 0.14	90.4 ± 25.2	8 ± 4
	5.1.5	954	Clay Loam	35 ± 9.4	0.30 ± 0.14	61.7 ± 16.25	8 ± 3
	5.1.6	4946	Clay Loam	50 ± 10.1	0.32 ± 0.13	41.5 ± 20.52	8 ± 6
	5.1.7	663	Clay	75 ± 16.3	0.34 ± 0.15	73 ± 25.25	8 ± 4
	5.1.8	2230	Loam	79.5 ± 16.5	0.27 ± 0.15	1.2 ± 1.10	8 ± 5
	5.1.9	2669	Clay Loam	62 ± 14.6	0.40 ± 0.13	65 ± 18.26	5 ± 3
	5.1.10	1755	Clay Loam	15.5 ± 13.2	0.43 ± 0.16	52.1 ± 25.36	5 ± 4
	5.1.11	906	Clay Loam	62 ± 15.3	0.28 ± 0.10	56.3 ± 26.35	5 ± 1
	5.1.12	638	Silt Loam	21.5 ± 14.3	0.30 ± 0.12	15 ± 10.25	5 ± 3
	5.1.13	421	Silt Loam	64.5 ± 15.4	0.40 ± 0.23	46 ± 25.36	5 ± 3
	5.1.14	1496	Clay Loam	34.5 ± 12.6	0.08 ± 0.02	18 ± 10.58	5 ± 4
	5.1.15	1562	Clay Loam	85 ± 15.4	0.43 ± 0.20	60 ± 20.54	5 ± 4
	5.1.16	1428	Clay Loam	103 ± 18.5	0.41 ± 0.16	21 ± 10.36	5 ± 4
	5.1.17	5471	Clay Loam	30 ± 15.4	0.14 ± 0.08	62.1 ± 25.24	10 ± 4
	5.2.1	2394	Clay Loam	22 ± 14.5	0.55 ± 0.12	4.2 ± 2.25	5 ± 3
	5.2.2	13303	Clay Loam	64 ± 17.5	0.28 ± 0.09	55.3 ± 24.35	22 ± 12
	5.2.3	675	Clay Loam	75 ± 24.7	0.28 ± 0.09	38.7 ± 26.34	5 ± 3
	5.2.4	230	Silty Clay Loam	75 ± 17.5	0.28 ± 0.07	91.8 ± 26.35	5 ± 2
6	6.1.1	1107	Clay Loam	95 ± 18.8	0.29 ± 0.04	28 ± 18.24	10 ± 4
	6.1.2	1855	Clay Loam	43 ± 15.9	0.36 ± 0.10	65 ± 24.36	8 ± 5
	6.1.3	3137	Silty Clay Loam	21.5 ± 18.7	0.27 ± 0.12	4.1 ± 2.12	8 ± 3
	6.1.4	2379	Clay Loam	28 ± 10.5	0.57 ± 0.14	48 ± 28.36	8 ± 7
	6.1.5	2065	Loam	97 ± 8.6	0.23 ± 0.16	66.6 ± 32.58	13 ± 6
	6.2.1	11667	Clay Loam	78 ± 8.8	0.40 ± 0.2	21 ± 10.89	25 ± 15

5: River Alluvial plain; 5.1: Kupal river Alluvial plain with slope less than 0.02% with different physicochemical properties (5.1.1–5.1.17); 5.2: Jarahi river Alluvial plain with slope less than 0.02% with different physicochemical properties (5.2.1–5.2.4); 6: Low Land; 6.1: Sharifieh wetland with high salinity and no vegetation cover with different physicochemical properties (6.1.1–6.1.5); 6.2: Mansouri wetland with high salinity and halophyte cover.

by the gravimetric method (Fig. 3). Also, were used a GARMIN eTrex 10 GPS device and Landsat 8 satellite images with path 165 and row 38 (five images corresponding to ground sampling days for February 12, March 16, April 17, May 19 and June 4 for 2019).

Methods and Stages of the Satellite Processing:

The flowchart of the method and steps of the study is shown in Fig. 4.

Pre-processing of Satellite Images

In this study, necessary corrections, including conversion of spectral value to radiance (Eq. (1)) and the atmospheric correction, were applied using the QUAC[7] technique. QUAC is an atmospheric correction that requires only approximate specification of sensor band locations. It uses a scene approach, and thus, it is faster than are corrections with first principle radiative models [15]. Also, to extract information from satellite images, the average wavelength was recorded for each band.

$$L_\lambda = \text{Gain} * \text{DN} + \text{Offset}. \quad (1)$$

Where, L_λ is the cell value as radiance, DN is the cell value digital number, Gain is the gain value for a

[7] Quick atmospheric correction

Fig. 2. Views of the dust hotspot of the southeastern Ahvaz in Khuzestan province.

specific band and Offset is the bias value for a specific band [24].

Fusion Images

In this study, to investigate the capability of fusion images in the soil moisture content mapping, the panchromatic and multispectral bands of Landsat 8 were combined by the Gram Schmidt Spectral Sharpening method [19, 24]. The Pan-sharpening algorithms are used to sharpen multispectral data using high spatial resolution panchromatic data, also the Gram-Schmidt method uses the spectral response function of a given sensor to estimate data.

NDMI (Normalized Difference Moisture Index)

The normalized moisture difference index or NDMI was calculated by near-infrared and middle infrared bands based on Equation (2) [17, 24]. In the present study, the 5 and 6 bands of Landsat 8 satellites were used as NIR or near-infrared band and Shortwave Infrared band or SWIR, respectively.

$$\mathrm{NDMI} = (\mathrm{BAND5} - \mathrm{BAND6})/(\mathrm{BAND5} + \mathrm{BAND6}) \quad (2)$$

It should be noted that Band 5 (NIR) is the recipient of water reflection in plants, and Band 6 (SWIR) is essential for identifying marshlands and distinguishing them from arid lands due to the strong absorption by water in this spectrum. Additionally, Bands 5 and 6 of the Landsat OLI sensor have a spatial resolution of 30 meters and a panchromatic band of 15 meters. The index was calculated for both originals bands and fusion bands (using a Band 8) [2].

Soil Moisture Content Model using Satellite Imagery

Understanding the relationship between variables is essential to creating statistical models. Using the indicators, the relationship between the variables can be realized. Here, was used the linear regression modeling, which is one of the methods of extracting information and evaluating satellite image data are between the ground parameters and the corresponding image [21]; The dependent variable is topsoil moisture content, and the independent variables are NDMI index (with the original (main) bands and integrated bands). Finally, the coefficient of determination (R^2) was calculated.

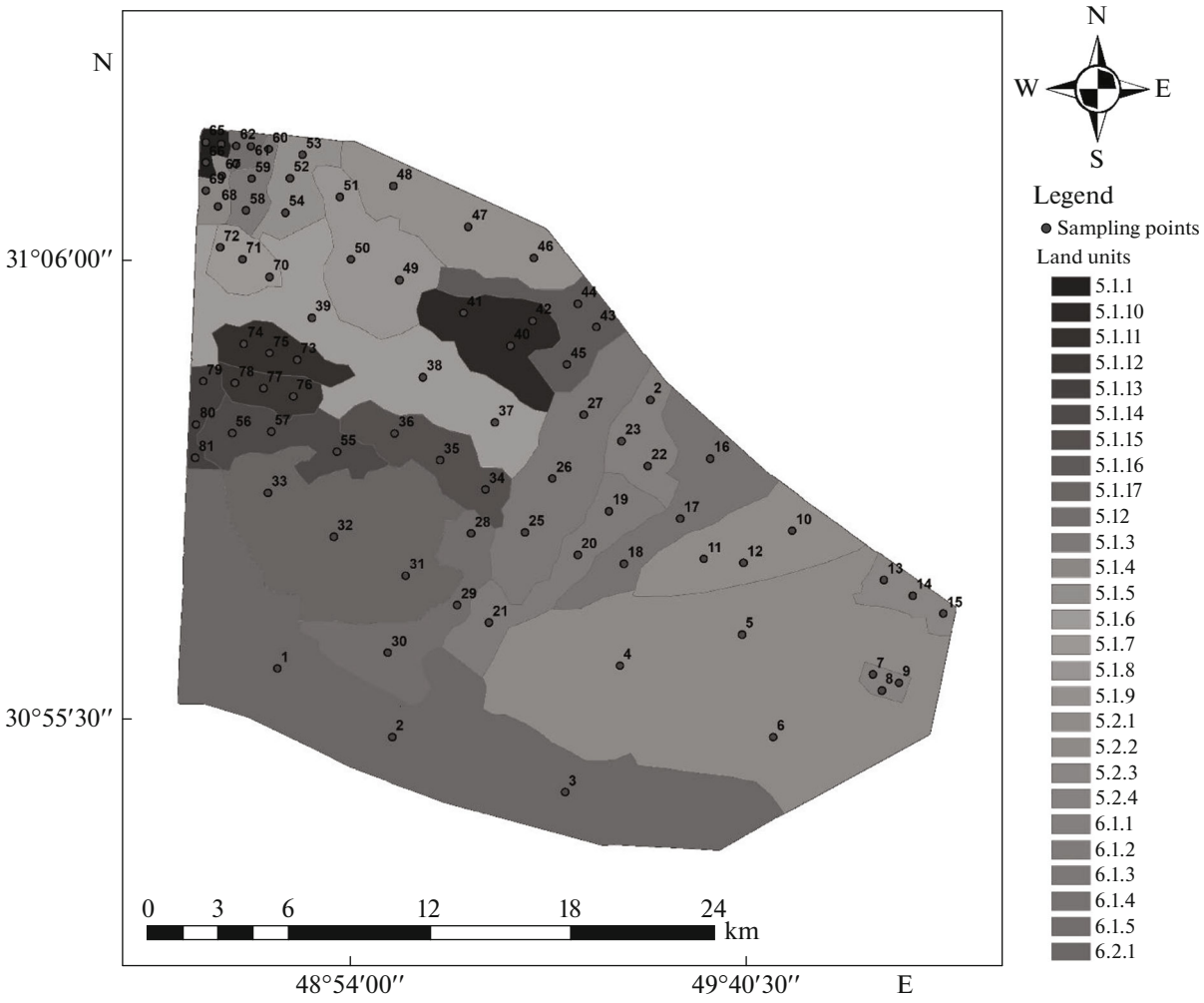

Fig. 3. Map of land units (described in Table 1) in the case study and position of sampling points.

Validation and Evaluation Criteria

In order to evaluate the performance of the models, the statistics of Root Mean Square Error (RMSE), Mean Absolute Error (MAE), and the coefficient of determination (R^2) were obtained from the following equations (3), (4), and (5):

$$\mathrm{RMSE} = \sqrt{\frac{\sum_{i=1}^{n}(p_i - o_i)^2}{n}}, \quad (3)$$

$$\mathrm{MAE} = \sum_{i=1}^{n}\frac{|p_i - o_i|}{n}, \quad (4)$$

$$R^2 = \frac{\left[\sum_{i=1}^{n}(P_i - \bar{P})(O_i - \bar{O})\right]^2}{\sum_{i=1}^{n}(P_i - \bar{P})^2\sum_{i=1}^{n}(O_i - \bar{O})^2}. \quad (5)$$

In the above equations, p_i and o_i are estimated and observed of the topsoil moisture content values, respectively; and $\bar{O}$ and $\bar{P}$ are the mean of the observed and estimated the topsoil moisture content values, respectively, and n, is the number of samples. The determination coefficient (R^2) is a dimensionless criterion, whose best value is one. It is suggested that MAE and RMSE could be used as criteria to include both the validation and accuracy [24].

Topsoil Moisture Content Map

Finally, after assessing the resulting models of topsoil moisture content index for the main (original) and fusion images for each month, the best model was selected and applied for the topsoil moisture content map.

RESULTS AND DISCUSSION

Main The statistical summary of the soil properties studied is shown in Table 2. The results demonstrate

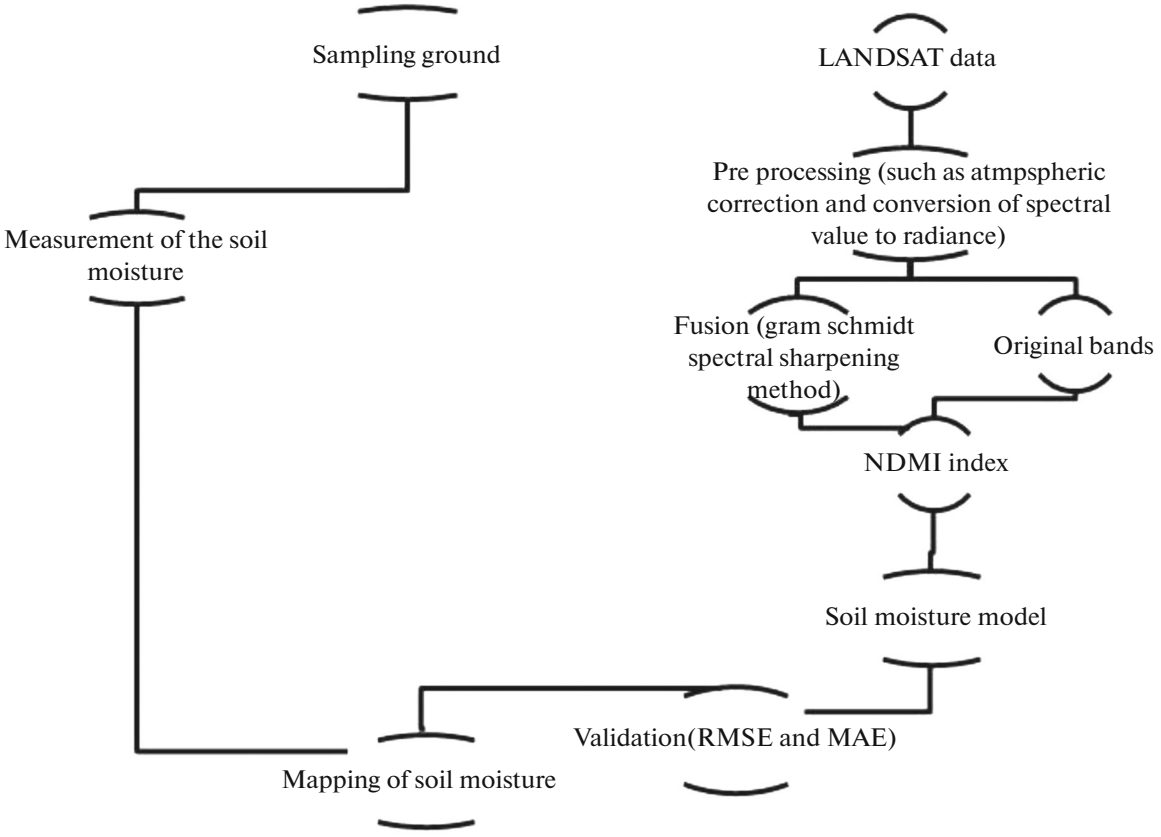

Fig. 4. Flowchart of research methods.

that among the soil chemical properties, the sodium absorption ratio has the highest coefficient of variation (47%) compared to other parameters. The presence of Mishan and Gachsaran geological formations, which consists of alternating layers of anhydrite, marl and salt, causes salinity of soils, in the study area [1]. Moreover, the shallow water table in some parts of the area has caused high solubility chemicals compounds such as sodium chloride to accumulate on the soil surface due to the evaporation process. Also, the average

Table 2. Summary of statistics (maximum, minimum, mean and coefficient of variations, CV) for soil properties

Property	Minimum	Maximum	Mean	SD	CV
SAR	7.98	227	98.28	68.34	47.53
OM, %	0.01	0.82	0.34	0.19	0.1
$CaCO_3$, %	9	51.5	19.65	6.25	1.98
EC, dS m^{-1}	1.8	134	70.68	33.83	16.19
pH	6.82	8.2	7.4	0.27	0.01
Sand, %	13.5	66.5	43.26	10.23	2.42
Silt, %	7	61	37	8.49	1.94
Clay, %	9	51.5	19.65	6.25	1.98
Bulk density, g cm^{-3}	1.4	1.60	1.52	0.12	0.10
MWD, mm	2.14	6.68	4.63	0.95	0.196
PWP, %	6.01	24.02	15.62	4.24	1.15

MWD: mean weight diameter of dry aggregates, SAR: sodium absorption ratio, OM; organic matter, EC: electrical conductivity, PWP: permanent wilting point, the number of observation points is 243 points ($n = 243$) (that included in 27 units' land * three points * three replications).

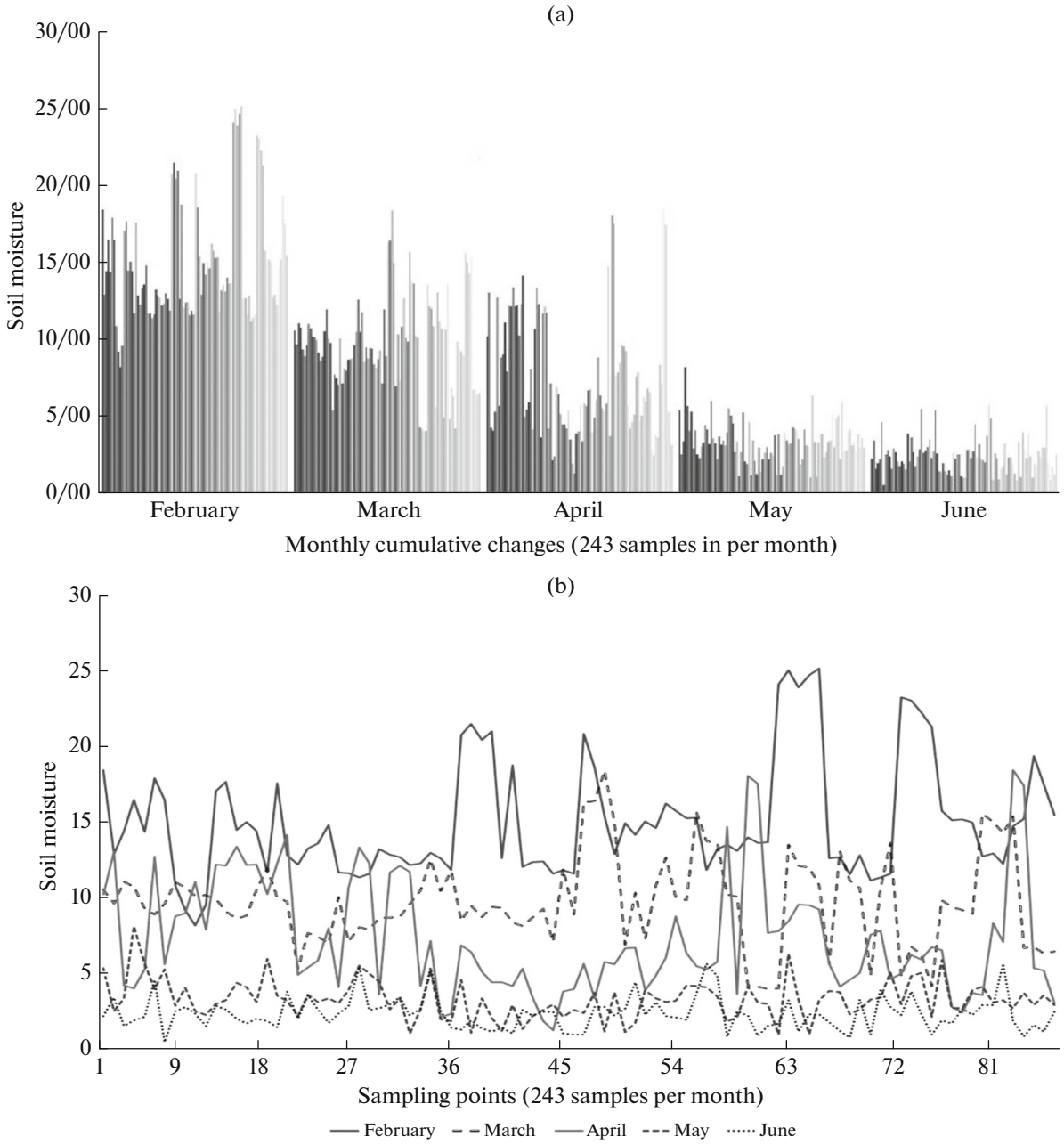

Fig. 5. The trend of cumulative changes in soil moisture content (a) and Percentage of soil moisture content obtained for sampling points per month (b).

organic matter in the soils (0.34%) indicates that these soils are poor in the organic matter. Furthermore, the percentage of $CaCO_3$ has a wide range, and its maximum and minimum are 51.5 and 9%, respectively. The average $CaCO_3$ in the region is 19.65%. Soil pH has the most minor variability compared to other parameters, varying from 6.82 to 8.2. The predominant textures of the soil were Clay and Clay loam, and among the soil particle components, clay particles had the highest variability.

The percentage of the topsoil moisture content obtained in the sampling points is shown in Fig. 5, according to which the difference in moisture between the minimum and maximum can be due to the type and texture of the soil in different areas and the difference in the evapotranspiration of each of these areas.

Also, after using the Gram Schmidt Spectral Sharpening method, the spatial resolution was improved. Figure 6 shows a visual comparison for February, as an example.

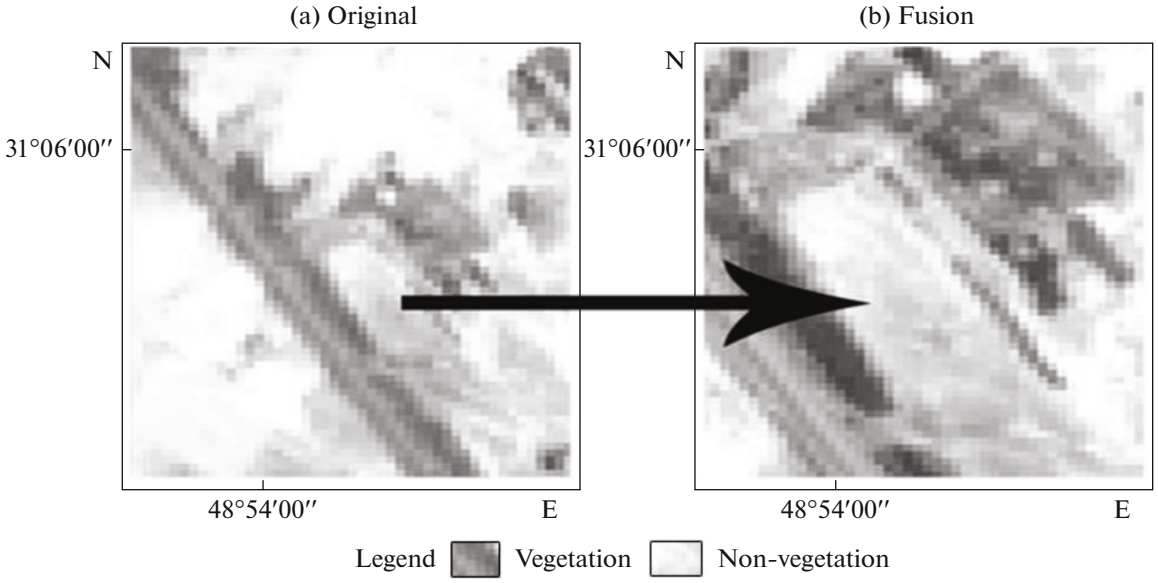

Fig. 6. Increase the spatial resolution of the fusion images for February 2019. Fig. (a) introduces the original image, and Fig. (b) demonstrate the fusion image.

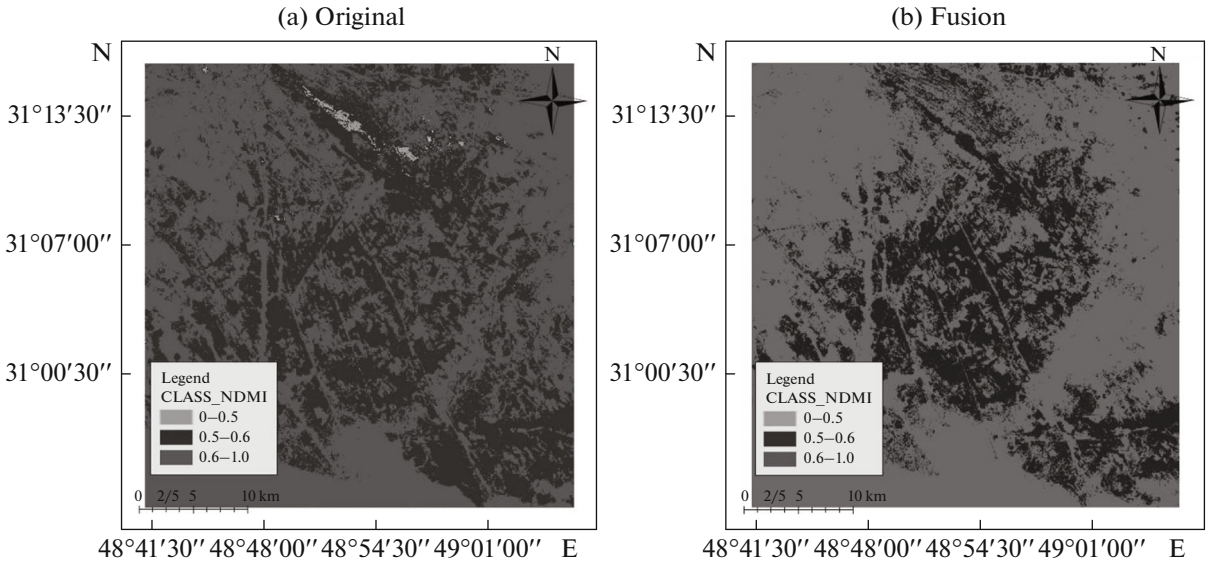

Fig. 7. NDMI map for February 2019 (original and fusion model).

Also, the results of merging panchromatic images and multispectral bands for February, March, April, May, and June are given in Tables 3 and 4. Furthermore, in Table 4, the Y and X variables are the estimated moisture content and the NDMI index, respectively. The following is a map of the NDMI index in Figs. 7 to 11.

The results obtained from the linear regression model between topsoil moisture content and NDMI index for different months are given in Tables 3 and 4, respectively. According to the results in Table 4, the highest determination and Pearson's coefficients were related to April month, with R^2 and Pearson's coefficient values of 0.564 and 0.543, respectively, which

Table 3. Pearson correlation coefficient values between topsoil moisture and NDMI index

Month	Model	Variables effective	Pearson coefficient
February	1	NDMI-Original Bands	0.413
	2	NDMI-Fusion Bands	0.199
March	3	NDMI-Original Bands	0.443
	4	NDMI-Fusion Bands	0.154
April	5	NDMI-Original Bands	0.543
	6	NDMI-Fusion Bands	0.291
May	7	NDMI-Original Bands	0.399
	8	NDMI-Fusion Bands	0.280
June	9	NDMI-Original Bands	0.483
	10	NDMI-Fusion Bands	0.503

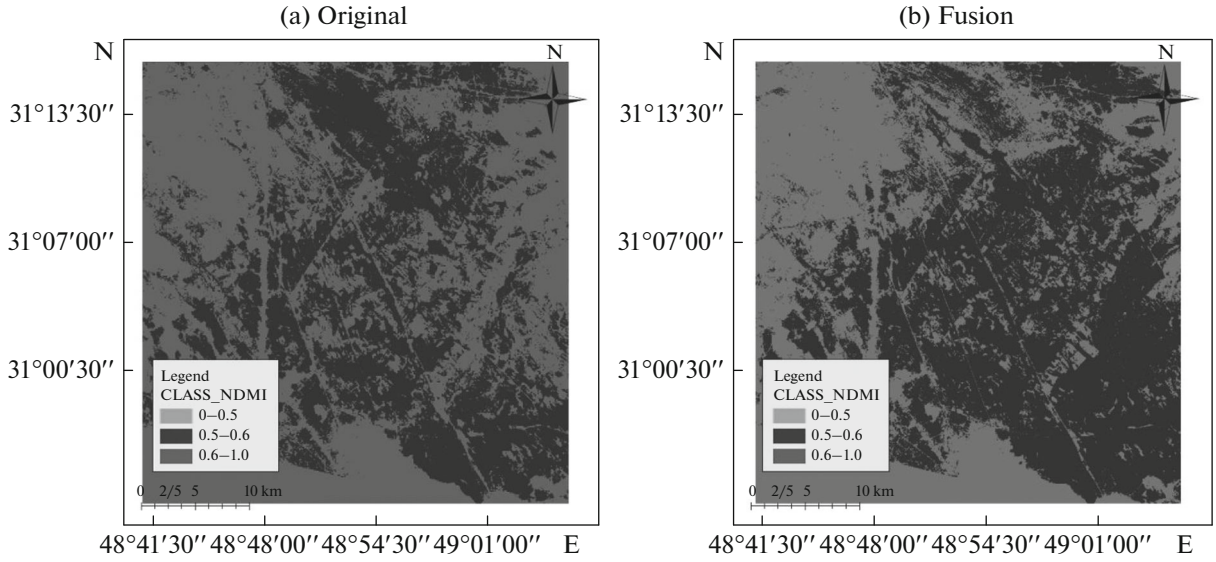

Fig. 8. NDMI map for March 2019 (original and fusion model).

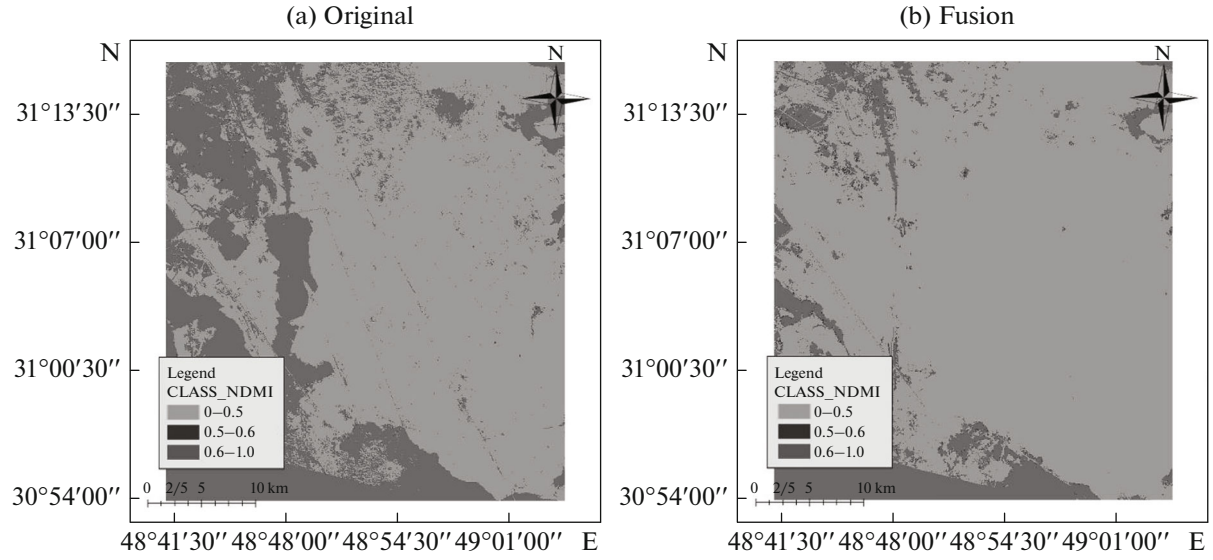

Fig. 9. NDMI map for April 2019 (original and fusion model).

Table 4. Linear regression results for the data obtained from the main band and fusion and model obtained

Month	Data Type	Model*	Sig	R^2
February	Original Bands	$Y = 69.304*(X) - 24.709$	0.04	0.307
	Fusion Bands	$Y = 67.001*(X) - 25.700$	0.03	0.303
March	Original Bands	$Y = 46.321*(X) - 35.858$	0.01	0.352
	Fusion Bands	$Y = 70.778*(X) - 51.653$	0.04	0.068
April	Original Bands	$Y = 331.616*(X) - 23.942$	0.004	0.564
	Fusion Bands	$Y = 174.731*(X) - 1.962$	0.04	0.168
May	Original Bands	$Y = 13.811*(X) - 3.582$	0.01	0.463
	Fusion Bands	$Y = 38.703*(X) - 4.344$	0.046	0.037
June	Original Bands	$Y = 45.596*(X) - 23.156$	0.048	0.101
	Fusion Bands	$Y = 126.465*(X) - 3.279$	0.003	0.467

* The Y and X variables are the estimated moisture content and the NDMI index, respectively. The "Sig" is significance. Also, the linear model diagram for April (the best estimated model) is presented in Fig. 12.

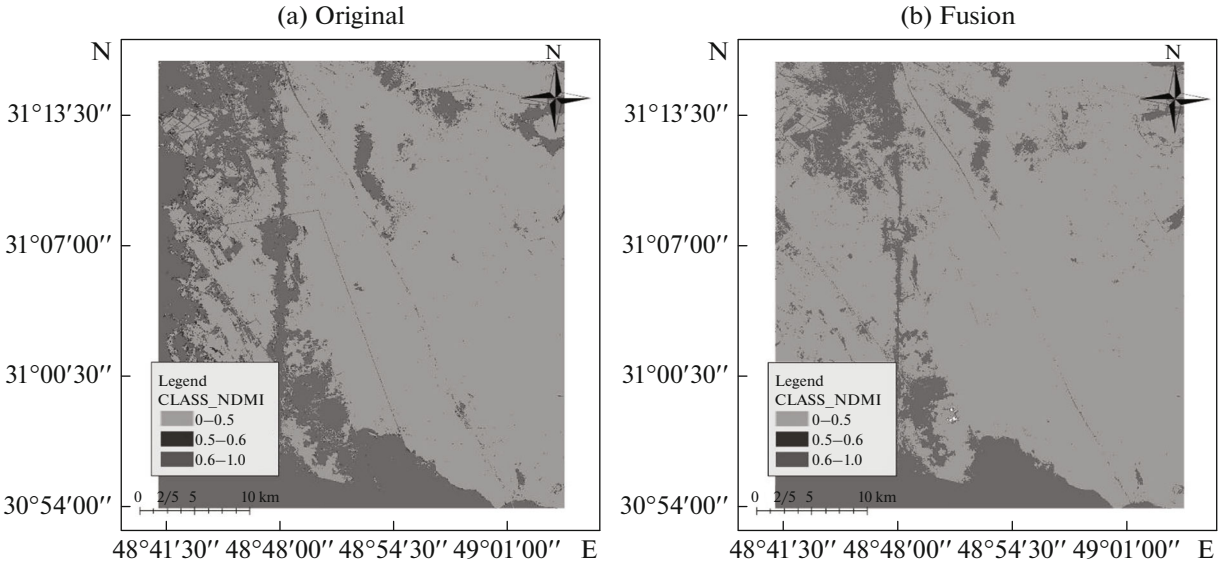

Fig. 10. NDMI map for May 2019 (original and fusion model).

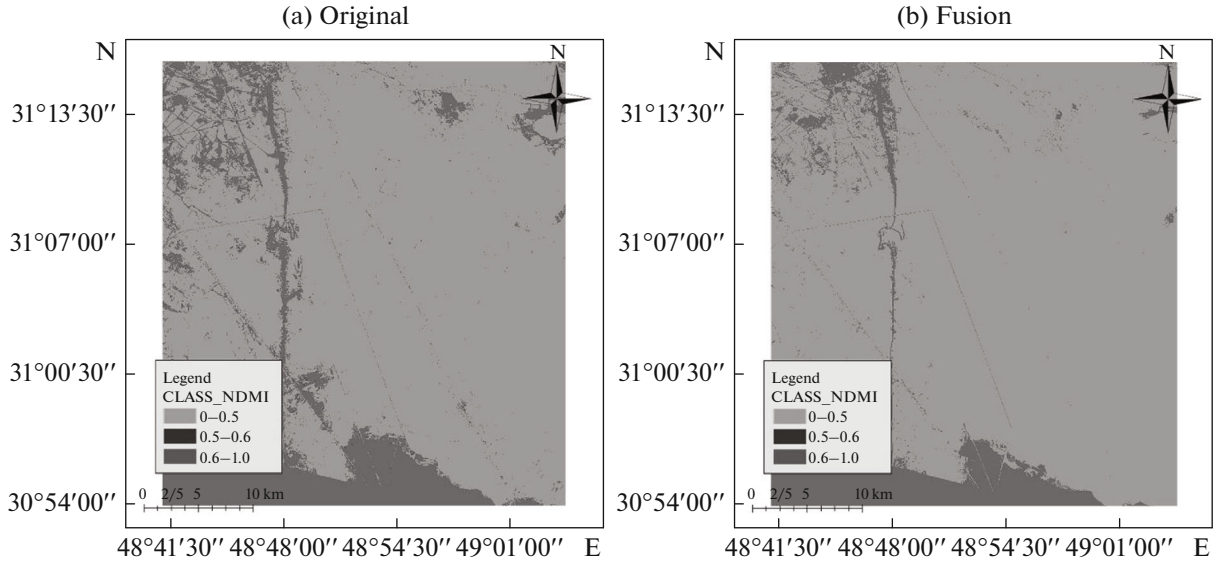

Fig. 11. NDMI map for June 2019 (original and fusion model).

showed a positive correlation. Based on the criteria of determination coefficient (Table 4) and accuracy statistics of models (Table 5), only one estimated model, for April month, among the ten estimated models was selected as the best model to prepare the final soil moisture content map (Fig. 12). The validation results are shown in Table 5, based on it were estimated the values of root mean error or RMSE and mean absolute error value or MAE.

Based on the criteria of validation of the estimated models (Table 5). Finally, the model obtained for April month with an R^2 above 0.56, and the least RMSE and MAE criteria, 1.25 and 5.45, respectively, was selected as the best estimation model to prepare the final soil moisture content map. Also, it was found that in most estimation models (4 months out of 5 months modeled), the main (original) models have higher accuracy in simulation than the fusion models (with the Band 8 or panchromatic Band) (except in the June month estimation model). Based on the validity of the estimated models, the best regression model was chosen to prepare the final map for April month, which is shown in Table 4 and Fig. 12.

According to the results of Table 6, it was found that the estimated average percentage of soil surface

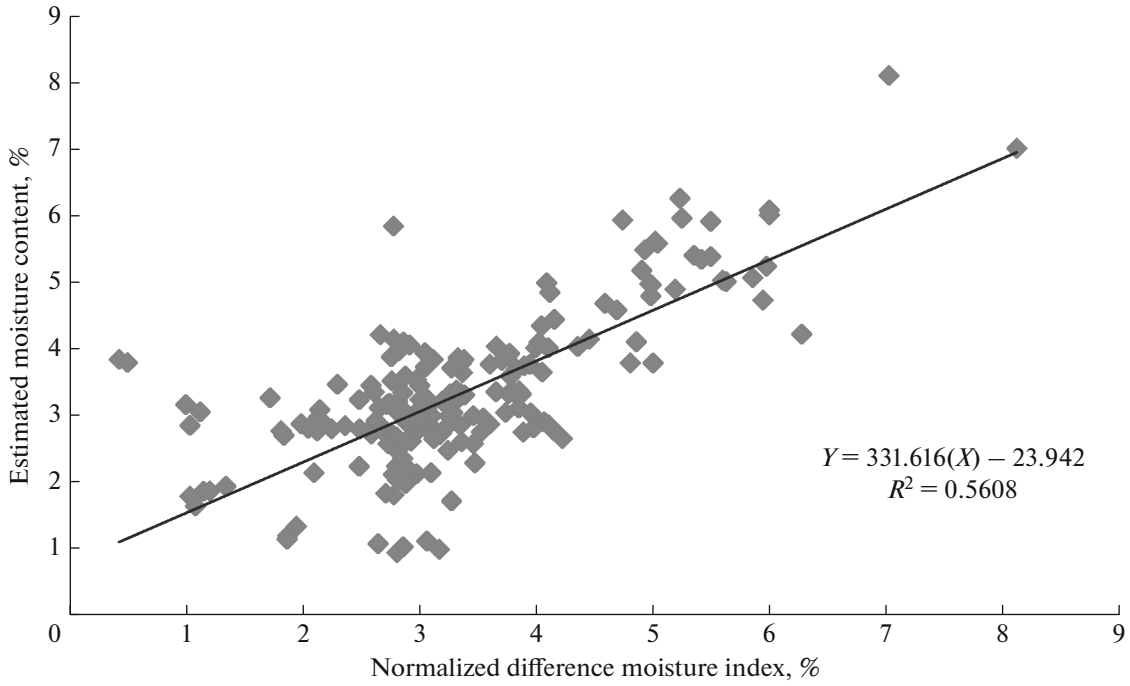

Fig. 12. Linear model graph for the data obtained for April (the best estimated model).

Table 5. Accuracy statistics in estimated models of topsoil moisture content percent for each month (sample size, 243)

Month	Model number	RMSE (percent)	MAE (percent)	Standard deviation
February	1	7.55	8.25	3.96
	2	15.71	14.11	11.80
March	3	1.97	6.47	1.08
	4	10.51	30.35	3.69
April	5	1.25	5.45	0.51
	6	6.281	38.36	2.94
May	7	4.061	13.47	1.88
	8	9.07	44.82	3.80
June	9	1.41	10.18	0.62
	10	5.70	6.77	4.72

Table 6. Percentage of area of each topsoil moisture content class in different months

Class	February	March	April	May	June
<2%	0	6.63	0.22	0.02	3.49
2–4%	71.67	0.03	0.76	86.08	60.89
4–8%	20.42	4.65	43.05	13.78	35.62
8–12%	7.81	27.61	25.7	0.04	0
>12%	0.09	61.08	30.29	0.08	0

moisture during different months in the region has been a decreasing trend (Fig. 5). After producing the moisture content maps in different months, changes in topsoil moisture content in the region were classified into five classes, which included areas less than 2%, 2 to 4%, 4 to 8%, 8 to 12%, and more than 12% (Fig. 13). Based on this, February to June months, respectively, shows the highest to lowest percentage of top soil moisture content (Table 6).

DISCUSSION

In the present study, Landsat 8 images with normalized difference moisture index (NDMI) showed good accuracy to assess soil moisture content due to the use of NIR and SWIR values to detect water reflections in plants and soil surface moisture (which was consistent with the studies Koohbanani et al., [13], and Yuan et al., [21]. This issue can be attributed to reason increasing the soil surface moisture, leading to decreased reflectance from the soil, which indicates the soil moisture content is an intense light absorbed in some wet months. In addition, the changes of soil spectral reflectance with water content in the SWIR band was significantly more prominent than in the visible band (this is consistent with the results Yuan et al., [21]. It should be noted that based on Khanmohammadi and Homaee [12], when the topsoil moisture content is less than 50%, short infrared bands can better reflect soil moisture content. Also, according to the estimated model's error table (Table 5), it was determined that the Fusion models showed less accuracy than the orig-

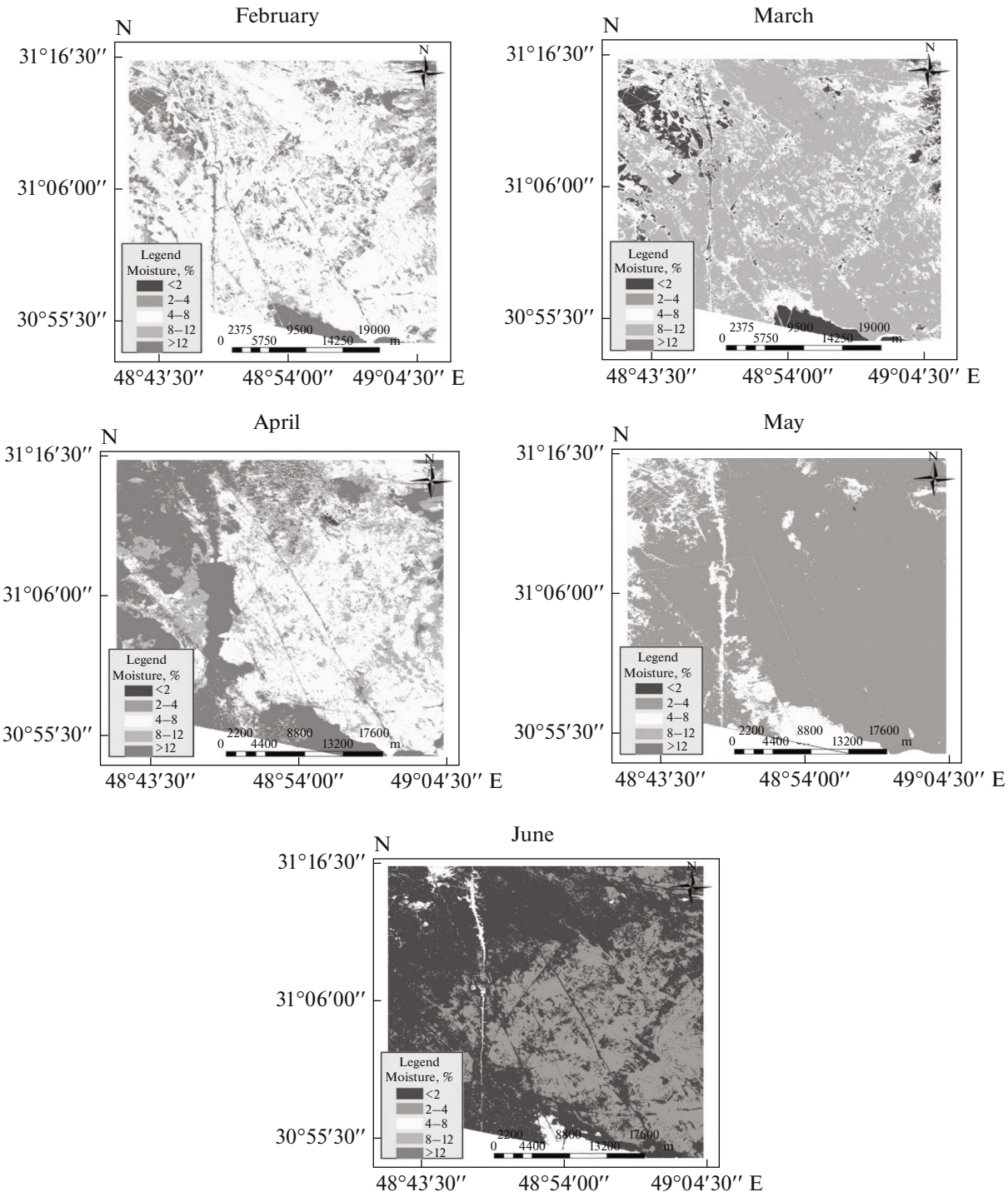

Fig. 13. The final map of topsoil moisture content estimated in the study area for other months of 2019.

inal models (original Bands), in most months of the year (RMSE = 3.24, MAE = 8.63), and finally, the soil moisture content maps were performed with the original models (temporarily and spatially). Table 6, also calculates the area percentage for each moisture class in different months. On the authority to the result, March has the highest percentage in the upper class of 12% (61.08), which according to the rainy season in the region, indicates the accuracy of the conclusions. Most of the percentage of area in the dry season is in the 2–4% classes (86.08 and 60.89 respectively for May and June). The results indicated that the NDMI index could be considered an appropriate indicator for topsoil surface moisture in desert regions with poor vegetation (similar to Koohbanani et al. (2018) research).

CONCLUSIONS

Accurate monitoring of surface soil moisture content is an essential factor in the proper management of water, soil and vegetation resources and the prevention of dust in critical areas of arid regions. The aim of this study was to the assessment of the capability of satellite images in determining topsoil moisture content in the dust hotspot of south-eastern Ahvaz in Iran, and evaluate the topsoil moisture content by remote sensing indices. In this area, soil moisture content due to scarce and irregular precipitation and frequent drought is unavailable to the plant, and the vegetation cover is poor. Due to livestock traffic in this area, soil bulk density has increased (Table 2), and water holding capacity has decreased [6]. The difference in the topsoil moisture values (maximum and minimum values) for each month can be due to the type and texture variations of the soil in different regions and also the difference in the permeability of soils. After preparing topsoil moisture content maps for different months, their correlation was examined with ground values (observed data). Also, topsoil surface moisture content changes from February to June have a decreasing trend (Fig. 5). So, from February (9.73–15.02) to June (2.36–7.37), there was a sharp decrease due to sharp rainfall decrease in the study area on June. These findings are in agreement with Zand-Parsa et al., [22] results. In this study, the topsoil moisture content was determined using Landsat 8 satellite images, and its map was obtained using regression models. Therefore, by knowing the relationship between topsoil moisture content and wind erosion threshold in the region, the dust phenomenon can be predicted. Also, due to the fact, that topsoil moisture content in the study area is meager, especially in the warm months of the year, this issue can cause wind erosion. Therefore, it is suggested that measures be taken to improve the topsoil moisture content, such as restoration of vegetation (planting halophyte plants and the native to the area (such as, *Tamarix passerinoides*, *Lycium depressum* and *Seidlitzia rosmarinus* [1]), and upgrading rangeland species) and proper management of water resources in this region.

FUNDING

This research has been obtained from the cooperation of the scientific thesis team the master of science student (Mr. Farid Hezarian) in the field Soil Science Engineering, in University of Agricultural Sciences and Natural Resources of Khuzestan, Iran.

CONFLICT OF INTEREST

The authors declare that they have no conflicts of interest.

REFERENCES

1. H. R. Abbasi, *Identification Land Sensitivity to Wind Erosion in Khuzestan Dust Sources, Technical Report* (Research Institute of Forests and Rangelands, Iran, 2021), p. 97 [In Persian].
2. P. Asgarzadeh, H. Darvishi Boloorani, A. Bahrami, and S. Hamzeh, "Comparison between land surface temperature estimation in the single and multi-channel method using Landsat images 8," J. RS GIS Nat. Resour. **7** (3), 18–29 (2016) [In Persian].
3. M. BaniHabib, S. Najafi, and M. Portabari, "Investigating the causes of dust in the west and south of the country with focusing on the reasons for the drying of Hur al-Azim wetland and provide solutions to revive it," in *Proceedings of 6th National Conference on Water Resourced Management, Kurdistan, Iran, 2016* [In Persian].
4. R. Dehghani Bidgoli, H. Koohbanani, A. Keshavarzi, and V. Kumar, "Measurement and zonation of soil surface moisture in arid and semi-arid regions using Landsat 8 images," Arabian J. Geosci. **13**, art. 826 (2020). https://doi.org/10.1007/s12517-020-05837-2
5. M. Entezari, M, Esmaeily, and S. A. Niazmardi, *Estimation of Soil Moisture Content and Earth's Surface Temperature Using Landstat-8 Satellite Data*, The International Archives of the Photogrammetry, Remote Sensing and Spatial Information Sciences, Vol. **XLII-4**/W18, 2019 [In Persian].
6. Z. Ghorbani, S. Jafari, and B. Khalilmoghadam, "The effect of soil physicochemical properties under different land use on aggregate stability in some part of Khuzestan province," Electron. J. Soil Manage. Sustainable Prod. **3** (2), 29–51. (2013) [In Persian].
7. G. H. Hasanzade and D. Fazeli, "Dust and its environmental consequences, case study: (dust and its effects on respiratory and heart diseases in Ilam province)," *Proceedings of Iranian National Conference on Environmental Research, Hamedan, Iran, 2013* (Shahid Mofteh Univ., Hamedan, 2013), pp. 12–11 [In Persian].
8. P. Heidarian, A. Azhdari, M. Jodaki, J. Darvishi Khatooni, and R. Shhbazi, "Identifying of interior sources of dust storms using remote sensing, GIS and geology (case study: Khuzestan province)," Sci. Q. J. Geosci. **27** (105), 33–46 (2017).
9. B. Khalilmoghadam, M. Afyuni, K.C. Abbaspour, A. Jalalian, and A. Dhegihan, "Estimation surface soil shear strength by pedo-transfer functions and soil spatial prediction functions," J. Water Soil (Agric. Sci. Technol.) **25** (1), 187–195 (2011) [In Persian].
10. B. Khalilimoghadam and M. Bagheri Bodaghabadi, "Factors influencing the relative recovery rate of dunes fixed under different sand-fixing measures in southwest Iran," Catena **194**, art. 104706 (2020). Doi: . https://doi.org/10.1016/j.catena.2020.104706
11. B. Khalilimoghadam, S. A. Siadat, A. Yusefi, and K. Negaresh, "Atmospheric particle adsorption rates of plants in an industrial city of southwest Iran," Aeolian Res. **53**, art.100752 (2021).
12. F. Khanmohammadi and M. Homaee, "Soil moisture content estimating with NDVI and land surface temperature and normalized moisture index using MODIS images," J. Soil Water Resour. Prot. **2** (4), 45–37 (2014) [In Persian].
13. H. Koohbanani and M. Yazdani, "Mapping the moisture of surface soil using Landsat 8 imagery (case study:

suburb of Semnan city)," Geogr. Sustainability Environ. **28**, 65–77 (2018) [In Persian].

14. M. S. Le and Y. A. Liou, "Spatial-temporal assessment of surface moisture and evapotranspiration variability using remote sensing techniques," *Remote Sens.* **13**, art. 1667 (2021) https://doi.org/10.3390/rs13091667
15. D. Moravec, J. Komárek, M. López-Cuervo, S. Medina, and I. Molina, "Effect of atmospheric corrections on NDVI: inter comparability of Landsat8, Sentinel-2, and UAV sensors," Remote Sens. **13**, art. 3550 (2021).
16. S. Nakhainejad Fard, H. Gholami, D. Akbari, M. Telfer, and M. Rezaei, "Evaluation of different image integration algorithms in preparing plant index maps," J. Geogr. Inf. **28** (112), 199–217 (2018).
17. N. Poornazari, B. Khalilimoghadam, Z. Hazbavi, and M. Bagheri Bodaghabadi, "Land degradation assessment in the dust hotspot of south-eastern Ahvaz, Iran," Land Degrad. Dev. **32**, 896–913 (2021). doi.org/ https://doi.org/10.1002/ldr.3748
18. H. Rajab Pour, Master Thesis (Kerman Shahid Bahonar Univ., 2013) [In Persian].
19. K. S. Rawat, S. K. Singh, and P. Kumar, "Synergetic methodology for estimation of soil moisture content over agricultural area using Landsat-8 and Sentinel-1 satellite data," Remote Sens. Appl. Soc. Environ. **15** (2019).
20. A. Şekerte kin, A. Murat Marangoz, and S. Abdikan, "Soil moisture content mapping using Sentinel-1A synthetic aperture radar data," Int. J. Environ. Geoinformatics **5** (2), 178–188 (2016).
21. J. Yuan, X. Wang, C. X. Yan, S. R. Wang, X. P. Ju, and Y. Li, "Soil moisture content retrieval model for remote sensing using reflected hyperspectral information," *Remote Sens.* **11**, art. 366 (2019). https://doi.org/10.3390/rs11030366
22. Sh. Zand-Parsa, S. Parvizi, A. R. Sepaskhah, and M. Mahbod, "New method for estimating hydraulic parameters by measuring soil moisture content in the field," J. Soil Water Sci. **22** (1), (2017) [In Persian].
23. H. Zolfaghari and H. Abedzadeh, "Synoptic analysis of dust systems in western Iran," Geogr. Dev. **15** (6) 173–187 (2015) [In Persian].
24. A. Zoratipour and M. Firoozynejad, "Investigating the changes in LST, NDVI, NDMI Indicators using MODIS images in Ahwaz," *Proceedings of 13th National Conference on Watershed Management Science and Engineering of Iran, 2018* (Mohaghegh Ardabili Univ., 2018) [In Persian].